Statistical mechanics of strong and weak point vortices in a cylinder

By OLIVER BÜHLER

School of Mathematics and Statistics, University of St Andrews,
St Andrews KY16 9SS, United Kingdom

(Received 17. Apil 2002)

The motion of one-hundred point vortices in a circular cylinder is simulated numerically and compared with theoretical predictions based on statistical mechanics. The novel aspect considered here is that the vortices have greatly different circulation strengths. Specifically, there are four strong vortices and ninety-six weak vortices, the net circulation in either group is zero, and the strong circulations are five times larger than the weak circulations. As envisaged by Onsager [Nuovo Cimento **6** (suppl.), 279 (1949)], such an arrangement leads to a substantial amplification of statistical trends such as the preferred clustering of the strong vortices in either same-signed or oppositely-signed pairs, depending on the overall energy level. To prepare the ground, this behaviour is illustrated here first by a simple toy model with exactly solvable statistics. A microcanonical ensemble based on the conserved total energy E and angular momentum M for the whole vortex system is then used, in which the few strong vortices are treated as a subsystem in contact with a reservoir composed of the many weak vortices. It is shown that allowing for the finite size of this reservoir is essential in order to predict the statistics of the strong vortices accurately. Notably, this goes beyond the standard canonical ensemble with positive or negative temperature. A certain approximation is then shown to allow a single random sample of uniformly distributed vortex configurations to be used to predict the strong vortex statistics for all possible values of E and M. Detailed predictions for the energy, two-vortex and radial distribution functions of the strong vortices are then made for comparison with three simulated cases of near-zero M and low, neutral, or high E. It is found that the statistical mechanics predictions compare remarkably well with the numerical results, including a prediction of vortex accumulation at the cylinder wall for low values of E.

I. INTRODUCTION

The application of statistical mechanics to two-dimensional point vortex dynamics was first suggested by Onsager[1] in a landmark paper in 1949, in which he sketched a possible explanation for the formation of coherent vortices on statistical grounds linked to the possibility of negative (statistical) temperatures for point vortex systems in a bounded domain. Onsager's suggestions have continued to attract some interest because two-dimensional fluid dynamics is a relevant paradigm in many applications such as geophysical fluid dynamics (in which the large-scale quasi-horizontal flow along stratification surfaces in the atmosphere or oceans is approximately layerwise two-dimensional), or plasma dynamics under certain conditions[2]. Indeed, a successful application of statistical mechanics to problems in these fields suggests a hidden degree of predictability that could easily be obscured by conventional direct numerical simulations. Such statistical predictability can be exploited quantitatively at much lower computational cost than by the brute force simulations of ensembles of many individual flow realizations. This is a compelling vision if one considers, for example, the hugely expensive geophysical climate and weather simulations, for which currently only a very small ensemble of direct simulations at very low resolutions is feasible. Statistical theories based on Onsager's ideas (and on others that go beyond the point vortex idealization) have already been used successfully for predicting the detailed behaviour of certain idealized geophysical flow problems[3]. Formidable obstacles remain in order to make such theories applicable in practice, but the potential rewards are great.

Onsager described his ideas only in qualitative form and the detailed theoretical exploration of these issues only began with the development of a mean-field theory by Montgomery and Joyce[4,5] which has since been extended and refined mathematically in many ways over the years[6–9]. Accurate direct numerical simulations of point vortices over long times have become feasible over the last two decades[10,11]. It was suggested[11] that for geophysical applications the most relevant values for the number of vortices N lie in an intermediate range between the regime of low-dimensional chaos (where N may be less than 10) and the 'thermodynamic' regime in which $N \to \infty$ in some subtle limit. This point of view is also taken here, where only cases with $N = 100$ are studied.

Now, the topic of the present paper goes back to a suggestive remark made by Onsager concerning the characteristic appearance of vortex distributions in a negative temperature state, and which to my knowledge has not been considered explicitly since. In his masterful succinct exposition, Onsager says that in such a state

"...vortices of the same sign will tend to cluster,—*preferably the strongest ones*—, so as to use up excess energy at the least possible cost in term of degrees of freedom ...the weaker vortices, free to roam practically at random, will yield rather erratic and disorganised contributions to the flow" (my italics).

This encapsulates two crucial insights: (a) that strong vortices will be more predictable than weak ones; and (b) that the maximum disorder of the flow as a whole (which is implied by the statistical theory) will be achieved in a remarkably inhomogeneous, composite manner, in which the relative order of the strong vortices will be more than compensated for by the increased disorder of the weak ones. The present paper is an attempt to verify and exploit both of these insights in the simplest possible setting that allows comprehensive numerical and theoretical exploration.

To the best of my knowledge, detailed previous studies have all focused on the case of identical (or nearly identical[11]) absolute vortex circulations, or on the even more restricted case of identical vortex circulations throughout. In these cases, the statistical behaviour of the flow is in some sense directly determined by the constraint of fixed total

energy: large energy values must require the coming together of same-signed vortices, and vice versa for low energy values (see II below). In other words, the occurrence of vortex clusters is then enforced directly by the total energy constraint. However, once different vortex strengths are present there is scope for interestingly different behaviour, in which some vortices cluster spontaneously whilst others do not.

The plan for the paper is as follows: §II introduces the main features of the studied Hamiltonian point vortex system and corrects some minor errors in related works; §III briefly illustrates Onsager's suggestion by an analogy with a simple toy model, which serves to prepare to ground for the vortex theory; §IV presents direct numerical simulations of the vortices; §V derives statistical mechanics predictions and applies these to the simulations; and some concluding remarks are given in §VI.

II. HAMILTONIAN POINT VORTEX DYNAMICS

The Hamiltonian form of the equations of motion for N point vortices with circulations Γ_i and instantaneous Cartesian coordinates $\boldsymbol{x}_i(t) = (x_i, y_i)$ (where $i = 1, 2, \ldots, N$) are:

$$\Gamma_i \frac{\mathrm{d}x_i}{\mathrm{d}t} = +\frac{\partial H}{\partial y_i}, \qquad \Gamma_i \frac{\mathrm{d}y_i}{\mathrm{d}t} = -\frac{\partial H}{\partial x_i}. \tag{II.1}$$

The pairs (x_i, y_i) are canonical phase space coordinates, with invariant phase space volume element $\mathrm{d}\boldsymbol{x}_1 \mathrm{d}\boldsymbol{x}_2 \ldots \mathrm{d}\boldsymbol{x}_N$. In the special case of a circular cylinder with radius R centred at the coordinate origin[6] the wall boundary condition is satisfied[12] by placing for each physical vortex at location $\boldsymbol{x}$ a single image vortex with opposite circulation at location $\boldsymbol{x}R^2/|\boldsymbol{x}|^2$. This leads to an invariant Hamiltonian $H(\boldsymbol{x}_1, \ldots, \boldsymbol{x}_N)$ as

$$H = -\frac{1}{4\pi} \sum_{i>j}^{N,N} \Gamma_i \Gamma_j \, \ln(r_{ij}^2) + \frac{1}{4\pi} \sum_{i=1}^{N} \Gamma_i^2 \, \ln(R^2 - r_i^2) + \frac{1}{4\pi} \sum_{i>j}^{N,N} \Gamma_i \Gamma_j \, \ln(R^4 - 2R^2 \boldsymbol{x}_i \cdot \boldsymbol{x}_j + r_i^2 r_j^2), \tag{II.2}$$

where $r_i^2 = x_i^2 + y_i^2$, $r_{ij}^2 = (x_i - x_j)^2 + (y_i - y_j)^2$, and the asymmetry in the logarithmic terms arises because the image vortices do not move with the implied physical velocity at their location. In other words, the circular cylinder wall cannot be removed. The double sums run over all pairs $i > j$, i.e. there are $N(N-1)/2$ individual terms in these. As $0 \leq r_i \leq R$, the phase space is clearly bounded and its volume is $(\pi R^2)^N$. In the generic case of Γ_i with different signs we clearly have $H \in (-\infty, +\infty)$ due to various combinations of terms with $r_i \to R$ or $r_{ij} \to 0$. Indeed, even at fixed $H = E$, say, individual terms in (II.2) can go to $\pm\infty$ whilst adding up to a finite number.

The first sum in (II.2) involves the usual free-space interaction term, which goes to $+\infty$ as $r_{ij} \to 0$ for same-signed vortex pairs, and vice versa for oppositely-signed dipoles. As is well known, this symmetric appearance masks a quite distinct dynamical behaviour in these two cases, with same-signed vortices orbiting each other whilst oppositely-signed ones propagating along a straight line. The second sum involves a self-interaction term for each vortex, which leads to counter-clockwise propagation at fixed r_i for $\Gamma_i > 0$ and vice versa for $\Gamma_i < 0$. Unlike the pair interaction terms, this term always goes to $-\infty$ as $r_i \to R$, which is linked to the ever-closer approach of the vortex to its oppositely-signed image in this limit. In other words, the cylinder wall is a location of infinite negative energy for each vortex. Finally, the third sum in (II.2) involves the interaction of each

vortex with the images of all other vortices. Its terms become singular only if $r_i, r_j \to R$ and $r_{ij} \to 0$.

One can note in passing that the dynamically active nature of the cylinder wall that is expressed by the self-interaction terms distinguishes the present case from the previously studied doubly periodic case[10,11]. These self-interaction terms add advection parallel to the wall to the dynamics, which somewhat enhances the mobility of individual vortices. Also, one can note that in the cylinder case propagating vortex dipoles split up when they approach the cylinder wall and then propagate along the wall into opposite directions. Unless they collide with other vortices beforehand, the vortices would then rejoin on the other side of the cylinder, and again enter the interior as a dipole. Such vortex behaviour might in fact be relevant for vortex dynamics on beaches, where the vicinity of the shoreline has a similar effect as the cylinder wall[13].

The infinities of the various terms in (II.2) occur on a set of measure zero in phase space volume, but they nevertheless have an impact on direct numerical simulations as well as on statistical theories, especially those with non-uniform phase-space measures (e.g. (II.3) below). Indeed, the possibility of negatively infinite self-interaction energy is important even in the simplest case $\Gamma_i = \Gamma = \text{const}$, although this seems to have been overlooked at times. For instance, Caglioti *et al.*[8] consider the conditions for existence of the usual canonical partition function Z defined by the total phase space integral

$$Z = \int \exp(-\beta H)\, \mathrm{d}\boldsymbol{x}^N, \tag{II.3}$$

where β is the usual parameter inversely proportional to the (statistical) temperature. They state that $Z < +\infty$ exists for fixed N and Γ if and only if

$$\beta \in \left(\frac{-8\pi}{\Gamma^2 N}, +\infty \right), \tag{II.4}$$

where the finite negative range is needed in order to bound the importance of same-signed vortex collisions with their infinite positive energies. However, this miscalculates the importance of the *negative* infinite energies as vortices approach the wall. Indeed, Z for a single vortex in a cylinder is easily evaluated as

$$Z = \frac{\pi}{1-\beta_*} R^{2(1-\beta_*)} \quad \text{only if} \quad \beta_* = \frac{\beta\Gamma^2}{4\pi} < 1, \tag{II.5}$$

otherwise $Z < +\infty$ does not exist. It seems that this implies that (II.4) in Caglioti *et al.* should be replaced by the slightly more symmetrical

$$\beta \in \left(\frac{-8\pi}{\Gamma^2 N}, \frac{+4\pi}{\Gamma^2} \right), \tag{II.6}$$

which exhibits a finite temperature range also for $\beta > 0$. (In the particular asymptotic limit subsequently studied in that paper[8], the re-scaled upper limit in (II.6) still tends to $+\infty$, so the subsequent results may well remain intact.)

Somewhat surprisingly, this means that a point vortex system with $\Gamma_i = \Gamma$ and bounded by a solid wall, if coupled to an infinite energy reservoir at positive temperature T, will collapse to the wall as T drops towards $\Gamma^2/4\pi$, where Boltzmann's constant has been set to unity. Some evidence for such behaviour is given in §V below. Of course, the point vortex model will lose its physical significance when this happens, i.e. the finite core and finite self-energy of physical vortices will become important in this limit. Also, any coupling to a *finite* energy reservoir will arrest the collapse (cf. §III).

Now, in the remainder of this paper the following set-up will be studied. The total

number of vortices $N = 100$ will be split into $N_A = 4$ strong vortices and $N_B = 96$ weak vortices with respective circulations

$$\Gamma_A = \pm 10\pi \quad \text{and} \quad \Gamma_B = \pm 2\pi. \tag{II.7}$$

The net circulation in either group is zero. This is a natural constraint for physical situations that have arisen from localized vortex forcing, which always produces vortex dipoles with zero net circulation[13]. These particular values have been chosen in order to focus on the most complex scenario, as follows.

Because absolute energy values in (II.2) are meaningless (unlike in most classical systems), the relevant measure of importance of the individual sums in (II.2) comes from considering their variance over the phase space. Neglecting $\Gamma_A\Gamma_B$ interaction terms between strong and weak vortices, it turns out (cf. §III below) that the total variance of the Γ_A^2 terms in the double sums scales approximately as $O(N_A^2\Gamma_A^4)$, and correspondingly so for the weak vortices. Therefore the parameters have been arranged such that these variances are approximately equal. The total variance of the Γ_A^2 self-interaction terms in (II.2) scales as $O(N_A\Gamma_A^4)$ and it turns out that for the chosen set-up the numerical prefactor makes this term significant in size compared with the term $O(N_A^2\Gamma_A^4)$. However, for the weak vortices the self-interaction variance $O(N_B\Gamma_B^4)$ is small compared to the term $O(N_B^2\Gamma_B^4)$. In summary, strong and weak vortices are expected to interact vigorously and the dynamics of the strong vortices is in addition significantly affected by the presence of the wall.

It remains to consider a second invariant that arises due to the azimuthal symmetry of the Hamiltonian H in (II.2), namely the invariant angular momentum

$$\hat{M} = \frac{1}{2\pi}\sum_{i=1}^{N}\Gamma_i\, r_i^2. \tag{II.8}$$

There are no other invariants, so vortex motions with $N > 2$ are presumably non-integrable in the cylinder. Unlike H, the invariance of $\hat{M}$ is not robust in the sense that a small disturbance of the problem (say, perturbing the cylinder wall to be elliptical) would destroy the invariance of $\hat{M}$. Nevertheless, in the present case $\hat{M}$ clearly plays a rôle and needs to be considered formally on the same footing as H. It is straightforward to show that for the chosen set-up the strong and weak vortex contributions to the variance of $\hat{M}$ are again roughly equal.

Finally, it is noteworthy that in a set-up in which all the Γ_i are sign-definite, the conservation of $\hat{M}$ implies that the accessible phase space is bounded even without a cylinder wall, and this has been used to study negative temperature states of such a set-up using only the first term in (II.2). However, in the present set-up with Γ_i of either sign this cannot be done (contrary to assertions sometimes made[7,14], where (II.8) was misquoted with Γ_i replaced by Γ_i^2).

III. A SOLVABLE TOY MODEL

Here a toy model with exactly solvable statistical mechanics is discussed in order to prepare the ground for the statistical mechanics of the vortex system. The toy model is the one-dimensional Ising model without external magnetic field, which can be thought of as an assembly of independent switches. Let there be M switches and let each switch either be in an "up" or "down" position, with corresponding energy values $E_i = \pm\epsilon_i$, where $i = 1, 2, \ldots, M$ and the constants ϵ_i describe the individual strength of the switches. The finite-sized discrete state space of the system is formed by the 2^M different states of all

the switches. The total energy is

$$E = \sum_{i=1}^{M} E_i \quad \text{with range} \quad -\sum_{i=1}^{M} |\epsilon_i| \le E \le +\sum_{i=1}^{M} |\epsilon_i|. \tag{III.1}$$

The energy extrema correspond to exactly one state each, and it is clear that there are only a few states with energies near these extrema. This scarcity of states is of crucial importance for the statistical mechanics of this system. Now, in an analogy with vortex dynamics each of the M switches corresponds to one of the $O(N^2)$ interaction terms in the first sum in (II.2), the other sums being disregarded. Each ϵ_i then corresponds to a pairing $\Gamma_i\Gamma_j$, and the up/down switch positions correspond crudely to the variability of the logarithms. Surprisingly, it will turn out that this crude analogy can already explain a number of features of the vortex system.

III.1. *Canonical statistical mechanics*

We first imagine the system in contact with an infinite energy reservoir at temperature T and inverse temperature $\beta = 1/T$. The individual switch statistics are then independent from each other and hence it suffices to consider the ith switch in isolation. (The analogous statement is of course not true in the vortex system, which is a coupled N-body problem.) The probabilities for the switch to be in the up/down position are then equal to $\exp(\mp\beta\epsilon_i)/Z_i$ respectively, where the normalization constant is the partition function $Z_i = 2\cosh(\beta\epsilon_i)$. The resultant average switch energy U_i is

$$U_i = -\epsilon_i \tanh(\beta\epsilon_i), \tag{III.2}$$

which shows that there is no energy equipartition between the switches unless $\beta = 0$, and that regardless of the sign of ϵ_i a positive temperature corresponds to negative U_i and *vice versa*. The behaviour of the switch as a function of $\beta\epsilon_i$ is easily characterized: if $\beta|\epsilon_i| \gg 1$ (i.e. $T \to 0+$) we have $U_i \approx -|\epsilon_i|$ and the switches are increasingly locked into their low-energy positions. On the other hand, if $\beta|\epsilon_i| \to 0+$ (i.e. $T \to \infty$) the switches become increasingly disordered and U_i goes to zero. A corresponding scenario unfolds for $\beta < 0$, which shows that positive and negative temperature statistics are perfectly symmetric here. All this applies qualitatively to the vortex system as well, though the near-symmetry between positive and temperature states is lost there when considering a mean-field theory[4,5].

The switch fluctuations can be analyzed by considering the number $U_i/\epsilon_i = -\tanh(\beta\epsilon_i)$, which is the average switch position. (Identical conclusions are reached by considering the variance of the switch energy, which is equal to $-\partial U_i/\partial\beta = \epsilon_i^2/\cosh^2(\beta\epsilon_i)$.) Absolute values of this number near unity mark ordered, predictable behaviour, whereas absolute values near zero mark disorder and randomness. For uniform ϵ_i order increases as $|\beta|$ increases. Consider now the case of there being two distinct types of switches: strong and weak, respectively, such that $|\epsilon_A| > |\epsilon_B|$, in obvious analogy to the vortex set-up. Clearly, for the same value of β the behaviour of the strong switches is going to be more ordered than that of the weak switches, i.e. $|U_A/\epsilon_A| \ge |U_B/\epsilon_B|$, with equality holding only when $\beta = 0$. Indeed, if $|\epsilon_A| \gg |\epsilon_B|$ then the strong switches can exhibit significantly more order than the weak switches, which illustrates the first part of Onsager's remark.

This point about order/disorder can be made in another way by looking at the contributions to the entropy of the system that are made by the strong and weak switches, respectively. The usual expression for the entropy in the canonical formalism is

$$S_i = \ln Z_i + \beta U_i = \ln(2\cosh(\beta\epsilon_i)) - \beta\epsilon_i \tanh(\beta\epsilon_i). \tag{III.3}$$

The switch entropy $S_i(\beta\epsilon_i)$ is hence a positive even function of its argument with maximum $S_i(0) = \ln(2)$ at the origin, and with monotone decrease to zero with increasing $|\beta\epsilon_i|$. (At $\beta = 0$ and $\beta \to \pm\infty$ the value of S_i is compatible with the microcanonical definition of entropy as the logarithm of the number of permissible states.) Again, this means that at fixed β we have $S_A \leq S_B$, i.e. the strong switches contribute less to the entropy than the weak switches.

A dynamical interpretation of this remarkably composite, inhomogeneous entropy distribution is suggested by the alternative variational formulation of canonical statistical mechanics in terms of maximum (information) entropy at fixed mean energy. In this view, the strong switches tend to become more ordered, and hence contribute less to the entropy, because in doing so they absorb the right amount of energy to allow the weak switches to be as disordered as possible. This peculiar sharing-out of the energy leads a distribution of maximum total entropy, which then emerges as a truly composite, interactive feature of the system. This illustrates the second part of Onsager's remark.

III.2. *Microcanonical statistical mechanics*

We now turn to consider the microcanonical statistics of the toy model, in which the total energy is fixed at a certain value E such that only states with this energy value are permitted and all such states are then deemed equally likely. This is the proper setting in which to analyze numerical simulations at conserved energy under an ergodic approximation, and the formalism developed here will be directly relevant to the vortex dynamics discussed later.

The total energy constraint now couples the individual switch statistics. Specifically, a subset of switches now behaves like a subsystem in contact with a *finite* energy reservoir formed by the other switches, and the key question is to analyze the statistical mechanics of such a subsystem. To this end we split the M switches into a subsystem A and a "reservoir" B such that $M_A + M_B = M$ and $M_B \gg 1$, assuming from now on that $M \gg 1$ to begin with. We have

$$E = E_A + E_B \tag{III.4}$$

for all permissible states. The probability of a particular subsystem state with energy E_A is then proportional to the number of reservoir states with $E_B = E - E_A$. Now, the density of reservoir states per unit energy interval is that of a sum of $M_B \gg 1$ independent zero-mean random functions with finite variances, which by the central limit theorem can be approximated by the continuous function

$$p_0(E_B) = \frac{1}{\sigma_B\sqrt{2\pi}} \exp\left(\frac{-E_B^2}{2\sigma_B^2}\right), \quad \text{where} \quad \sigma_B = \sum_{i=1}^{M_B} \epsilon_i^2 \tag{III.5}$$

is the energy variance of the reservoir. The subscript 0 denotes that this probability corresponds to a uniform distribution over all possible states. For a particular subsystem state with E_A we therefore obtain the probability

$$\begin{aligned} \mathit{Prob}\{\text{subsystem state with } E_A\} &\propto p_0(E_B = E - E_A) \propto \exp\left(\frac{-(E-E_A)^2}{2\sigma_B^2}\right) \\ &\propto \exp\left(\frac{E\,E_A}{\sigma_B^2} - \frac{E_A^2}{2\sigma_B^2}\right), \end{aligned} \tag{III.6}$$

where a factor independent of E_A has been absorbed into the proportionality constant determined by normalization. This means that for small subsystem energies $E_A^2 \ll 2\sigma_B^2$ the relative probabilities are described by canonical statistics with an inverse temperature

$\tilde{\beta} = -E/\sigma_B^2$. We note in passing that if $|E_A| \ll |E_B|$ then $\tilde{\beta}$ agrees with the microcanonical definition of inverse temperature of the reservoir as the derivative of $\ln p_0(E_B)$ with respect to E_B.

Now, for larger subsystem energies the finite size of the reservoir is felt via the second term in (III.6), which decreases the likelihood of such states and marks the departure from canonical statistical mechanics for the subsytem. (Coincidentally, the statistics of a *single* switch in contact with the finite reservoir are precisely canonical, due to the symmetry of its two energy levels.) Also, one can note that the probability distribution (III.6) admits a somewhat unusual maximum-entropy formulation in which the subsystem information entropy is extremalized subject to *two* constraints, namely that of fixed average energy as well as fixed energy variance. It is straightforward to show that such a procedure leads to a probability $\propto \exp(-\tilde{\beta}E_A - \tilde{\gamma}E_A^2)$ for a subsystem state with energy E_A, in accordance with the structure found in (III.6).

The above shows how microcanonical statistical mechanics can be used to calculate the statistics of a subsystem in contact with a finite reservoir, even beyond the usual asymptotic limit $M_B \to \infty$, $E/M_B = O(1)$ in which canonical subsystem statistics would emerge. The important reservoir energy variance σ_B^2 in (III.5) enters the definition of $\tilde{\beta}$ and it also demarcates the finite size of the reservoir as felt by the subsystem. In analogy with the toy model and (III.5), the reservoir variance in the vortex system is proportional to $N_B^2\Gamma_B^4$, as was previously asserted.

IV. NUMERICAL SIMULATIONS

Direct numerical simulations of the vortex system set-up from §II are described and analyzed. The comparison with statistical mechanics predictions follows in §V.

IV.1. *Numerical model details*

The model integrates the dynamical equations derived from (II.1) and (II.2), i.e.

$$\frac{\mathrm{d}\boldsymbol{x}_i}{\mathrm{d}t} = \sum_{j=1,j\neq i}^{N} \frac{\Gamma_j/2\pi}{(\boldsymbol{x}_i - \boldsymbol{x}_j)^2}\,(y_j - y_i, x_i - x_j) + \sum_{j=1}^{N} \frac{\Gamma'_j/2\pi}{(\boldsymbol{x}_i - \boldsymbol{x}'_j)^2}\,(y'_j - y_i, x_i - x'_j) \tag{IV.1}$$

As noted in §II, each vortex has an image vortex with parameters

$$\Gamma'_j = -\Gamma_j, \quad \boldsymbol{x}'_j = \boldsymbol{x}_j \frac{R^2}{x_j^2 + y_j^2} \tag{IV.2}$$

to satisfy the wall boundary condition. Notably, the second sum in (IV.1) includes a self-interaction term with $j = i$. Strong and weak vortices were chosen as in (II.7) and for definiteness the cylinder radius $R = 5$. By re-scaling (IV.1) the present simulations can be mapped onto simulations with arbitrary finite R and Γ_B provided the ratio $|\Gamma_A/\Gamma_B| = 5$ remains the same.

The numerical model itself is a standard Runge–Kutta scheme of 4/5th order with adaptive timestep refinement. The integrations are performed with double precision and in cycles of $\delta t = 0.01$, using adaptive timestep refinement until the error is less than the tolerance set to 10^{-9}. No regularization of the equations for numerical purposes was needed, e.g. there was no near-field smoothing to prevent large velocities, and the unusually low error tolerance is required to integrate safely through intermittent episodes

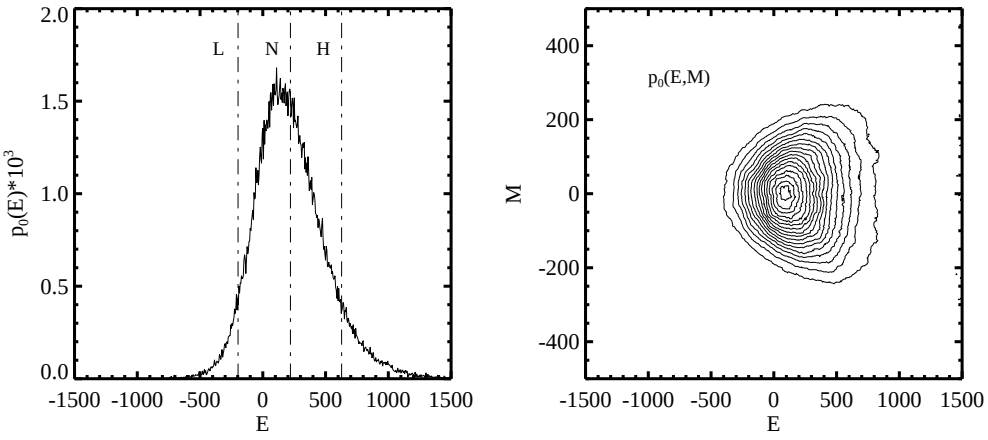

FIGURE 1. (a) Total energy pdf (based on 10^5 random samples with uniform distribution) with indications of the total energy levels for the Low, Neutral, and High runs. The average total energy is 222 with variance 284^2. (b) Joint total energy–angular momentum pdf, after some smoothing. The correlation coefficient between E and M is 10^{-3}.

in which vortices are getting very close to each other, or to the wall. These intermittent episodes lead to a model performance that can vary by a factor of ten over a run. The total energy and angular momentum are conserved with very high precision and all runs were performed on a single-processor workstation.

IV.2. *Description of three model runs*

Under the ergodic approximation the statistics of a run are determined by the invariant values of its Hamiltonian $H = E$ and its angular momentum $\hat{M} = M$, say. All runs had values of M very close to zero. This is because no exploration of the rôle of M was intended because of the non-robust nature of this invariant noted in §II. Three different energy values (denoted Low, Neutral, and High) were chosen to give runs broadly corresponding to regimes of positive, zero, and negative microcanonical temperature. The specific values for the three runs were

$$E = \{-197, 221, 628\}, \quad M = \{2.1, 4.1, 2.3\} \tag{IV.3}$$

and they were determined as follows[10]. A random population of 10^5 vortex configurations was generated in which each of the hundred vortices was placed independently with uniform probability anywhere inside the cylinder. The H values were then computed from (II.2) (this being the computationally expensive step) and a histogram was formed to give the probability density function (pdf) for the total energy $p_0(E)$, as plotted in figure 1a. The average energy is non-zero because of the sign-definite effect of the self-interaction terms in (II.2) and also because there are $O(N)$ more oppositely-signed terms than same-signed terms in the double sums. The corresponding pdf for the total angular momentum (not plotted) is close to a zero-mean normal distribution with variance equal to $\Gamma_i^2 R^4/48\pi^2$ summed over all vortices. Also plotted in figure 1b is the joint pdf of total energy and total angular momentum $p_0(E, M)$, which indicates approximate statistical independence of E and M.

At the begin of each run the four strong vortices were placed in the same positions, i.e.

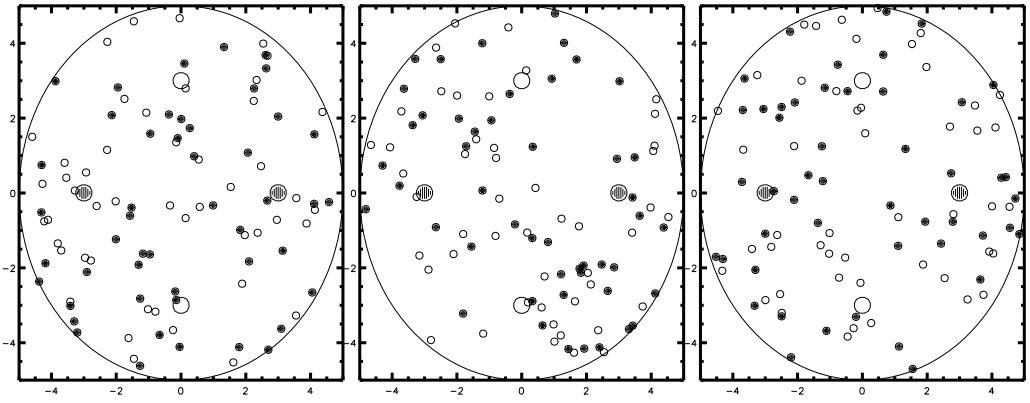

FIGURE 2. Inital states for the three runs with Low, Neutral, and High energy levels, from left to right. Large circles show the strong vortices, and black or white colour indicates positive or negative circulation.

these vortices were symmetrically spaced in azimuthal angle at a common radius $r = 3$, with alternating circulation from vortex to vortex. This is very close to an exact steady state of four vortices in a cylinder, which occurs at radius $r = (\sqrt{17} - 4)^{1/4} R \approx 2.96$, and hence the strong vortices are essentially set into motion by the weak vortices. The positions of the weak vortices were taken from uniformly distributed random samples that were generated until a sample with suitable E and M was found. The resulting initial states are displayed in figure 2. It is probably fair to say that it is impossible to guess by inspection of figure 2 whether and in what way the long-term statistics of the strong vortices will differ in these runs.

All runs were now integrated up to $t = 750$, which corresponds to many hundred cylinder traversals of each vortex, and 3000 instantaneous states of the evolution were stored at time intervals of $\Delta t = 0.25$. Very different behaviour of the strong vortices was observed. The low-energy run showed a strong tendency of vortices sticking close to the wall, or forming short-lived vortex dipoles. The high-energy run showed a strong tendency to form same-signed vortex pairs that persisted a comparatively long time. The neutral-energy run showed a mixture of both behaviours. In all cases there were fluctuations around this behaviour, but the self-organization of the vortices into these typical patterns was conspicuously clear.

Several quantitative diagnostics for the strong vortices were computed: their energy E_A (i.e. (II.2) evaluated using only the strong vortices), the distance between same-signed vortex pairs, and the distance between oppositely-signed vortex dipoles. The mean values and standard deviations of these quantities over the duration of the simulations are summarized in table 1, with pdfs presented in the next section. These numbers make clear that significant statistical differences are indeed observed between the runs. With increasing overall energy E the average of the subsystem energy E_A (which initially has equal value in all runs) increases and the average distance between same-signed vortex pairs decreases. Also, at the neutral energy level (with zero microcanonical temperature) there is no preference between pairing of same-signed or oppositely-signed vortices. The average distance between oppositely-signed vortex dipoles remains roughly constant as E is increased and close to a value corresponding to uniformly random placement of the

		Low	Neutral	High
Energy	E_A	-23 ± 126	141 ± 111	269 ± 136
predicted		-64 ± 136	129 ± 117	242 ± 152
Same-sign distance	r_{ij}	5.1 ± 2.1	4.5 ± 1.9	3.7 ± 2.0
predicted		5.1 ± 2.1	4.5 ± 1.9	3.9± 2.1
Opp.-sign distance	r_{ij}	4.5 ± 2.5	4.4 ± 2.1	4.6 ± 1.8
predicted		4.6 ± 2.5	4.5 ± 2.1	4.5 ± 1.9
Radius	r_i	3.6 ± 1.2	3.3 ± 1.1	3.1 ± 1.0
predicted		3.6 ± 1.2	3.3 ± 1.1	3.1± 1.1

TABLE 1. Mean values and standard deviations over the duration of the simulation vs. theoretical predictions for various quantities. For the distances r_{ij} and r_i these quantities are averaged over all relevant combinations of $i, j \in \{1, 2, 3, 4\}$ if $\Gamma_{1,2} = -10\pi$ and $\Gamma_{3,4} = +10\pi$.

vortices, which is 4.5 (with standard deviation 2.1). However, the standard deviation of this quantity reduces with E.

Table 1 also includes predictions based on the theory described in §V below. These predictions are generally quite accurate, except for E_A in the low-energy case and for the same-signed r_{ij} in the high-energy case. Sample autocorrelation functions based on the numerical time series feeding into these averages were computed in order to estimate confidence intervals. These suggested long-lived oscillations in the low-energy E_A with periods of about $t \sim 50$ as well as a slowly decaying autocorrelation in the high-energy r_{ij}, which presumably is linked to long-lived vortex pairs in that case. Confidence intervals based on these estimates put the observed discrepancies at the borderline of statistical significance.

V. COMPARISON WITH STATISTICAL MECHANICS

The numerical results are compared with pdfs estimated based on microcanonical statistical mechanics for the whole system. The general estimation procedure is described in some detail, not least because it contains an important *ad hoc* approximation that significantly reduces computational cost.

V.1. *Estimation of pdfs*

The estimation of pdfs is based on phase space densities $\rho(\boldsymbol{x}_1, \ldots, \boldsymbol{x}_N)$, which for convenience in the present case are normalized such that

$$\int \rho \, \mathrm{d}\boldsymbol{x}^N = 1, \tag{V.1}$$

where the integral is extended over the whole phase space. Relative to a chosen ρ the pdf of any phase space function $\Phi(\boldsymbol{x}_1, \ldots, \boldsymbol{x}_N)$ taking real values ϕ is defined as

$$p(\phi) = \int \delta(\Phi - \phi) \rho \, \mathrm{d}\boldsymbol{x}^N = \int_{\Phi=\phi} \frac{\rho \mathrm{dA}}{|\boldsymbol{\nabla}\Phi|}. \tag{V.2}$$

The scaling properties of the Dirac-δ function succinctly capture the thickness of the layers $\Phi \in [\phi, \phi + d\phi]$ measured in the surface integral on the right. Multiple pdfs $p(\phi_1, \phi_2)$ are defined analogously using products of δ-functions. Pdfs defined by (V.2) can be estimated numerically by forming histograms of $\Phi(\boldsymbol{x})$ based on random samples of $\boldsymbol{x}$. In theory, optimal convergence of such a procedure requires importance sampling, in which ρ

is used as the density of the random sample. In practice, using a uniform density coupled with histogram increments proportional to ρ is much cheaper in the present case of a finite phase space. The special case of a uniform density $\rho_0 = (\pi R^2)^{-N}$ is particularly important, for example $p_0(E)$ in figure 1 has been estimated from

$$p_0(E) = (\pi R^2)^{-N} \int \delta(H - E)\, \mathrm{d}\boldsymbol{x}^N. \tag{V.3}$$

All pdfs calculated from the uniform density are denoted by $p_0(\cdot)$.

The usual microcanonical density based on energy $H \in [E, E + dE]$ is defined as

$$\rho_E = \frac{\delta(H - E)}{\int \delta(H - E)\, \mathrm{d}\boldsymbol{x}^N} \tag{V.4}$$

and corresponding pdfs will be denoted by $p_E(\cdot)$. For simplicity, consideration of the angular momentum invariant is deferred until later. From (V.2) one obtains

$$p_E(\phi) \propto \int \delta(\Phi - \phi)\delta(H - E)\, \mathrm{d}\boldsymbol{x}^N \propto p_0(\phi, E), \tag{V.5}$$

up to an overall normalization factor. This means that $p_E(\phi)$ can in principle be evaluated from a joint pdf $p_0(\phi, E)$ based on the uniform distribution. However, for a particular value of E this is computationally very expensive, as most samples have to be discarded. On the other hand, if Φ depends only on a subset of the variables then its pdf can be much simplified, as follows.

Specifically, let $\boldsymbol{x}_A$ and $\boldsymbol{x}_B$ denote the coordinates of all the strong and weak vortices, respectively. Then $\mathrm{d}\boldsymbol{x}_A\mathrm{d}\boldsymbol{x}_B = \mathrm{d}\boldsymbol{x}^N$ and we consider only functions $\Phi(\boldsymbol{x}_A)$ from now on. From (V.5) one obtains

$$p_E(\phi) \propto \int \delta(\Phi - \phi) \left[\int \delta(H - E)\, \mathrm{d}\boldsymbol{x}_B \right] \mathrm{d}\boldsymbol{x}_A \propto \int \delta(\Phi - \phi)\rho_E(\boldsymbol{x}_A)\, \mathrm{d}\boldsymbol{x}_A, \tag{V.6}$$

where the integral in squared brackets is the marginal density $\rho_E(\boldsymbol{x}_A)$. Now, if it were the case that $H = H_A(\boldsymbol{x}_A) + H_B(\boldsymbol{x}_B)$ (as was true in the toy model) then

$$\rho_E(\boldsymbol{x}_A) \propto \int \delta(H_B + H_A - E)\, \mathrm{d}\boldsymbol{x}_B \propto p_0(E_B = E - H_A), \quad \text{where} \tag{V.7}$$

$$p_0(E_B) \propto \int \delta(H_B - E_B)\, \mathrm{d}\boldsymbol{x}_B \tag{V.8}$$

is the pdf of the weak vortex energy H_B in the uniform distribution. The last term in (V.7) means that the function $p_0(E_B)$ should be evaluated at $E_B = E - H_A$. Clearly, all states $\boldsymbol{x}_A$ with the same energy H_A are now equally likely. Because $\rho_E(\boldsymbol{x}_A)$ depends only on $E - H_A$ this is a huge simplification, as $p_0(E_B)$ can be computed once and for all from the uniform distribution.

However, the Hamiltonian (II.2) does not fit into this category, as we have

$$H(\boldsymbol{x}_A, \boldsymbol{x}_B) = H_A(\boldsymbol{x}_A) + H_B(\boldsymbol{x}_B) + H_I(\boldsymbol{x}_A, \boldsymbol{x}_B) \tag{V.9}$$

where the 'interfacial' energy H_I consists of terms involving both strong and weak vortex circulations. In principle, this means that $\rho_E(\boldsymbol{x}_A)$ does not depend solely on $E - H_A$. Calculating $\rho_E(\boldsymbol{x}_A)$ for all $\boldsymbol{x}_A$ directly would be very expensive, as even in the present case this would require a look-up table in eight dimensions. Instead, a much simpler *ad hoc* approximation for $\rho_E(\boldsymbol{x}_A)$ as a function of $E - H_A$ is used, which for $H_I = 0$ reduces to (V.7). The approximation is

$$\rho_E(\boldsymbol{x}_A) \propto p_0(E_R = E - H_A(\boldsymbol{x}_A)), \tag{V.10}$$

where

$$\boxed{p_0(E_R) \propto \int\int \delta(H_R - E_R)\,\mathrm{d}\boldsymbol{x}_A \mathrm{d}\boldsymbol{x}_B} \tag{V.11}$$

is the pdf of the 'reservoir' energy $H_R \equiv H_B + H_I$ based on the uniform distribution. Unlike in (V.8), the double integral is necessary here because H_R depends on both $\boldsymbol{x}_A$ and $\boldsymbol{x}_B$. This approximation effectively assigns the same probabilitiy to all states $\boldsymbol{x}_A$ that have the same strong vortex energy $H_A(\boldsymbol{x}_A)$. Indeed, the assigned probability can be shown to be the average probability over all states with the same H_A.

Based on this approximation, the pdf for any $\Phi(\boldsymbol{x}_A)$ is now given by

$$\boxed{p_E(\phi) \propto \int \delta(\Phi - \phi) p_0(E_R = E - H_A)\,\mathrm{d}\boldsymbol{x}_A}\,. \tag{V.12}$$

The pdf of H_A in particular simplifies further to

$$p_E(E_A) \propto p_0(E_A) p_0(E_R = E - E_A). \tag{V.13}$$

The additional consideration of the second (non-robust) angular momentum invariant (II.8) is straightforward, especially as $\hat{M} = \hat{M}_A + \hat{M}_B$ holds exactly. The microcanonical density becomes

$$\rho_{EM} = \frac{\delta(H - E)\delta(\hat{M} - M)}{\int \delta(H - E)\delta(\hat{M} - M)\,\mathrm{d}\boldsymbol{x}^N}, \tag{V.14}$$

the marginal density

$$\rho_{EM}(\boldsymbol{x}_A) \propto \int \delta(H - E)\delta(\hat{M} - M)\,\mathrm{d}\boldsymbol{x}_B, \tag{V.15}$$

and the joint 'reservoir' pdf based on the uniform distribution

$$\boxed{p_0(E_R, M_B) \propto \int\int \delta(H_R - E_R)\delta(\hat{M}_B - M_B)\,\mathrm{d}\boldsymbol{x}_A \mathrm{d}\boldsymbol{x}_B}\,. \tag{V.16}$$

The same approximation procedure for (V.15) as before then gives

$$\boxed{p_{EM}(\phi) \propto \int \delta(\Phi - \phi) p_0(E_R = E - H_A, M_B = M - \hat{M}_A)\,\mathrm{d}\boldsymbol{x}_A} \tag{V.17}$$

The predictions of the statistical mechanics theory are hence pdfs estimated based on (V.16) and (V.17). For comparison with figure 1 the functions $p_0(E_R)$ and $p_0(E_R, M_B)$ are plotted in figure 3.

Despite the somewhat opulent appearance of (V.16) and (V.17), the practical procedure for estimating pdfs is actually disarmingly simple. A sample of 10^5 states was generated using the uniform distribution and the corresponding values of $H, H_A, H_R, \hat{M}, \hat{M}_A, \hat{M}_B$ were computed and stored in lists, as were the coordinates $\boldsymbol{x}_A$ of the four strong vortices. Computing H is by far the most expensive step here. Histograms based on these lists were then used to estimate (V.16). For any function $\Phi(\boldsymbol{x}_A)$ to be investigated a corresponding list of values was then computed from the stored coordinates. This list together with a look-up table for the histogram increments $\propto p_0(E_R, M_B)$ at the shifted arguments was then used to estimate (V.17) at fixed E and M. It is worth stressing that only a single

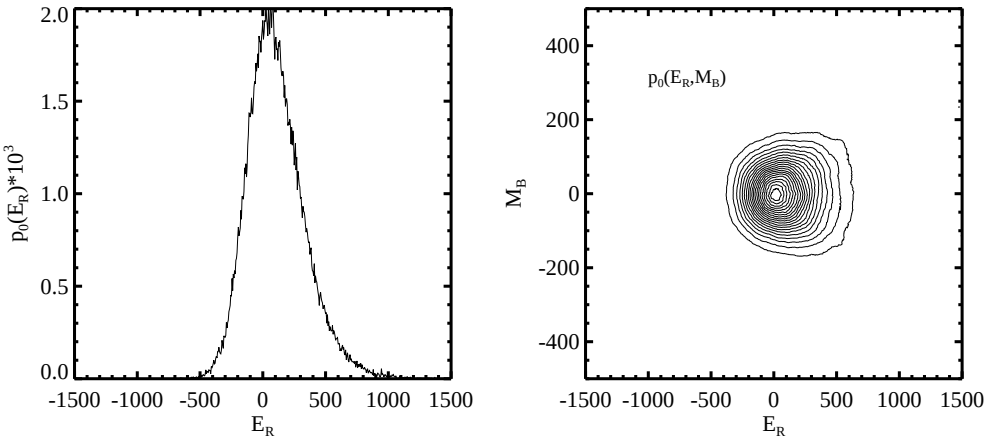

FIGURE 3. (a) Pdf of the reservoir energy $E_R = E - E_A$, where E_A is the energy of the strong vortices, based on 10^5 random samples with uniform distribution. The average reservoir energy is 109 with variance 229^2. (b) Joint reservoir energy–angular momentum pdf, after some smoothing, where $M_B = M - M_A$ and M_A is the angular momentum of the strong vortices.

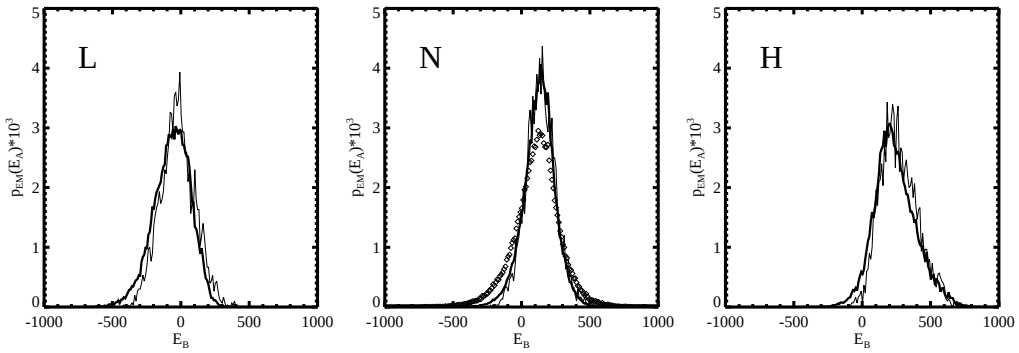

FIGURE 4. Pdfs of E_A, the energy of the strong vortices, for the three runs. Thin lines are simulation results, thick lines are theoretical predictions, and the squares denote $p_0(E_A)$.

large sample based on the uniform distribution is needed to describe the statistics of the system at arbitrary E and M.

V.2. *Comparison with model results*

The pdfs for E_A (i.e. the energy of the strong vortices) are plotted in figure 4. Throughout, thin lines denote pdfs estimated from histograms taken from the direct numerical simulations and thick lines denote theoretical predictions based on (V.17). Also shown in the middle panel is $p_0(E_A)$, which corresponds to random placing of the vortices with uniform distribution. As could be expected, in the neutral energy case this gives a reasonable first approximation, though still a less accurate one than $p_{EM}(E_A)$. The mean energy of the strong vortices increases as E increases and this can clearly be predicted quantitatively from the theoretical predictions. In most cases, there is very good agreement between the

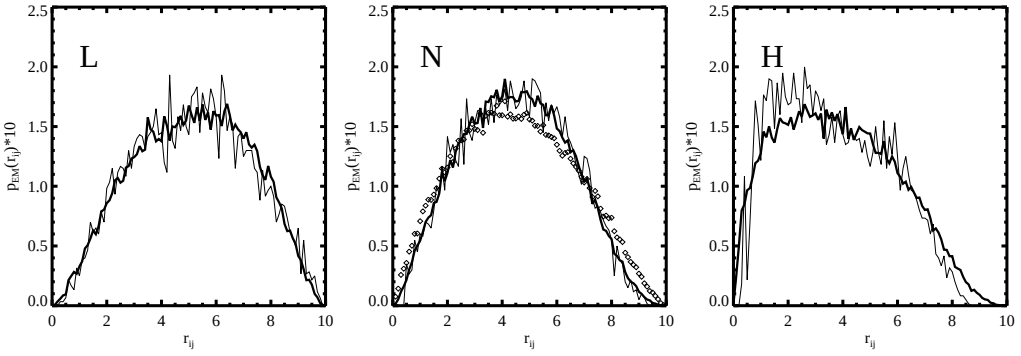

FIGURE 5. Pdfs of r_{ij} between strong vortices of the same sign, for the three runs. Thin lines are simulation results, thick lines are theoretical predictions, and the squares denote $p_0(r_{ij})$. The simulation results are averages over the pdfs of r_{12} and r_{34}.

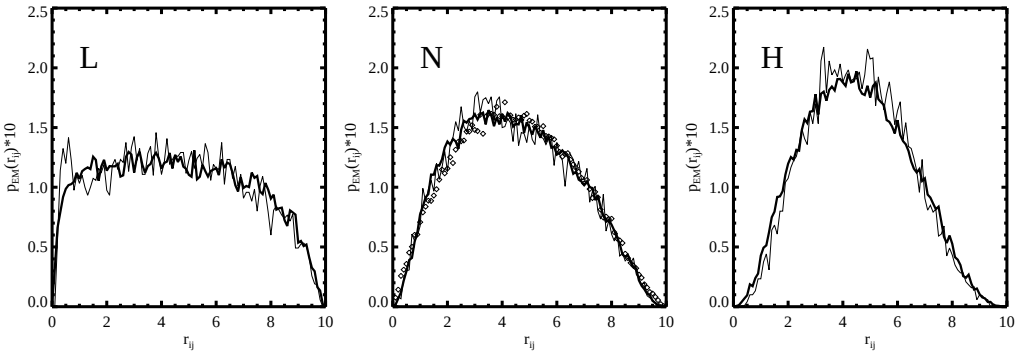

FIGURE 6. Pdfs of r_{ij} between strong vortices of opposite sign, for the three runs. Thin lines are simulation results, thick lines are theoretical predictions, and the squares denote $p_0(r_{ij})$. The simulation results are averages over the pdfs of r_{13}, r_{14}, r_{23}, and r_{24}.

theoretical and simulation statistics, not only in terms of accurate prediction of low-order moments, but also in the prediction of the non-Gaussian shape of the pdfs.

Figures 5-6 show the pdfs for the distance between same- and opposite-signed strong vortices, respectively. The tendency for same-signed vortices to cluster at smaller r_{ij} with increasing E is evident in figure 5. On the other hand, the indifference to E of the average r_{ij} between opposite-signed vortices that was noted in table 1 masks notable changes in the pdf that are evident in figure 6. These are well captured by the theoretical predictions.

Finally, figure 7 shows statistics for r_i, the vortex distance from the origin. This quantity is interesting due to the influence of the self-interaction terms in (II.2), which, as noted in §II, significantly affect the dynamics of the strong vortices. For neutral and high energies the pdf of r_i settles down to a shape quite close to the uniform distribution (except near the wall $r_i = R$), which is indicated by the squares in the middle panel. However, the first panel in figure 7 shows how the strong vortices tend to accumulate at the cylinder wall for very low energies. This is essentially a similar statistical effect as the formation of opposite-signed vortex dipoles in the first panel of figure 6, but the wall effect is clearly more pronounced in its pdf. Interestingly, the effective temperature estimated as $\mathrm{d}\ln p_0(E)/\mathrm{d}E$ from figure 1 at $E = -197$ gives ≈ 0.01 for this run. The the-

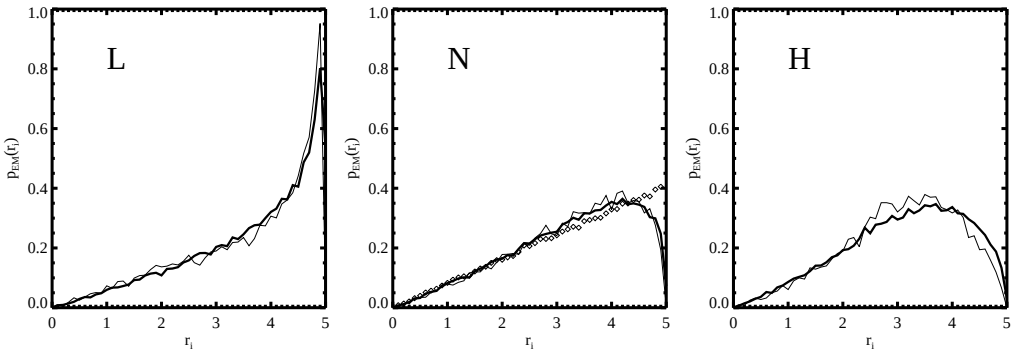

FIGURE 7. Pdfs of r_i, the distance from the origin of the strong vortices, for the three runs. Thin lines are simulation results, thick lines are theoretical predictions, and the squares denote $p_0(r_i)$. The simulation results are averages over the pdfs of r_1, r_2, r_3, and r_4.

oretical upper limit in (II.6) for the possible existence of canonical subsystem statistics in the present case gives ≈ 0.013, which confirms that this run is close to a collapse to the wall. Finite point vortex statistics in a collapse case would rely entirely on the finite size of the reservoir formed by the small vortices.

VI. CONCLUDING REMARKS

The theoretical predictions based on an ergodic approximation for the whole vortex system were seen to predict the pdfs of many, though not all, descriptive variables of the strong vortex subsystem with a surprisingly high degree of accuracy. Some simulation averages converged only very slowly and significantly longer integrations could test the quality of the ergodic approximation in these cases. On the other hand, non-ergodic observations might also be due to the crucial approximation leading to (V.17), which was necessary to estimate the theoretical pdfs at affordable computational cost. Otherwise, the prediction procedure was remarkably simple and cheap, relying only on a single random sample of vortex configurations to predict pdfs for *all* values of total energy E and angular momentum M.

The toy model, the direct numerical vortex simulations, and the theoretical predictions all corroborated Onsager's crucial insight that strong vortices will exhibit amplified statistical tendencies compared to weak vortices, and hence will be more predictable in a negative temperature state. It is the strongly unequal circulation strengths that allows the flow to organise itself in this inhomogeneous manner. It can be noted that in terms of entropy as a measure of accessible phase space volume, clustered vortices always present a low-entropy state. The crucial point is that in a negative temperature state the low entropy of the clustering strong vortices is more than compensated for by the high entropy of the freely roaming weak vortices.

It is intriguing to note that on the level of individual vortex dynamics there is a smooth transition from positive to negative temperature behaviour, exemplified by the smooth $p_0(E)$ in figure 1. By contrast, in a coarse-grained picture two vortices with opposite circulations that are close together cancel each other out and hence disappear from view. This illustrates why solutions to mean-field theories (such as the Sinh–Poisson equation[4]) have a characteristic cut-on behaviour as $\beta < 0$, because only same-signed vortex clustering is observable in the coarse-grained variables of these theories. It is also noteworthy that the near-collapse of the vortices to the wall in the present low-energy

case (which is linked to the theoretical upper bound in (II.6)) does not occur in the Sinh–Poisson equation because there the scaling has been arranged *ab initio* to render the wall-induced self-interaction energies negligible.

The present set-up seems to have been the most complicated to study, i.e. the strong vortices interact vigorously with both the wall and with the small vortices, and the small vortices themselves form only a finite energy and angular momentum reservoir. As noted before, the latter point puts the strong vortex statistics beyond the reach of the usual canonical theories. In other words, whilst the overall energy regime can be broadly classified by the sign of the usual statistical mechanics temperature, the temperature concept alone is not sufficient to make quantitative predictions. The modified maximum entropy principle suggested by the Gaussian pdfs of the toy model (in which entropy was maximized subject to both a fixed mean energy and a fixed energy variance) might allow analytical progress to be made here. Another possible avenue for future analytical progress is an asymptotic exploitation of the small parameter $|\Gamma_B/\Gamma_A|$.

It is tempting to generalize the present results (which directly apply only to well-separated finite-size vortices) to continuous vorticity distributions by letting $N \to \infty$ in some way. As is now well known, the relevant scaling must keep $N\Gamma = O(1)$ in this limit. However, this implies that the microscopic vortex mobility due to the induced velocity by the nearest vortices at average distance $\propto R/\sqrt{N}$ would decrease to zero as $\Gamma\sqrt{N} \propto 1/\sqrt{N}$. Therefore the microscopic vortex system equilibration time (which is implicitly assumed here to be small compared to the observation period) goes to infinity in this limit. This problem is directly observable, say, in the simplest case of many $\Gamma_i = \text{const.}$ vortices in a cylinder, for which exact solutions of the $N \to \infty$ limit are known[8]. Simulations starting from non-equilibrium initial conditions clearly show that these solutions are practically unattainable due the lack of vortex mobility. On the other hand, there is evidence[3] that the slow evolution of well-mixing large-scale flows can be approximated by statistical point vortex theory. Notably, random forcing also helps in this context, as it too increases the mobility of the vortex population. This suggests that a limit in which $N_A = \text{const.}$ and $N_B \to \infty$ could perhaps be used to model the behaviour of strong vortices surround by a sea of "filamentary vortex debris", because the stirring by the strong vortices could provide the essential mobility for the debris.

Finally, the prediction tools developed in this paper could be used to study an interesting 'inverse' problem: from observing only the strong vortices, can one deduce the number and strengths of the unobserved weak vortices? This would provide a nonlinear method for estimating unobservable sub-gridscale data, perhaps with applications in geophysical fluid dynamics.

ACKNOWLEDGEMENTS

The idea for the work grew out of a project undertaken at the 2000 summer study in Geophysical Fluid Dynamics hosted by the Woods Hole Oceanographic Institution (USA) and sponsored by the US National Science Foundation. Rick Salmon, the director of the 2000 summer study, is thanked for his support. Further financial support from the Nuffield Foundation (UK) under grant NAL/00034/G and from the Engineering and Physical Sciences Research Council (UK) under grant GR/R09565/01 is gratefully acknowledged. Ben Aschenbrenner is thanked for performing some early simulations.

References

[1]Onsager, L. 1949 Statistical hydrodynamics. *Nuovo Cimento (suppl.),* **6**, 279–287.
[2]Kraichnan, R. H., & Montgomery, D. 1980 Two-dimensional turbulence. *Rep. Prog. Phys.,* **43**, 547–619.
[3]Grote, M. J., & Majda, A. J. 1997 Crude closure dynamics through large scale statistical theories. *Phys. Fluids,* **9**, 3431–3442.
[4]Joyce, G., & Montgomery, D. 1973 Negative temperature states for the two-dimensional guiding-centre plasma. *J. Plasma Phys.,* **10**, 107–121.
[5]Montgomery, D., & Joyce, G. 1974 Statistical mechanics of "negative temperature" states. *Phys. Fluids,* **17**, 1139–1145.
[6]Pointin, Y. B., & Lundgren, T. S. 1976 Statistical mechanics of two-dimensional vortices in a bounded container. *Phys. Fluids,* **19**, 1459–1470.
[7]Eyink, G. L., & Spohn, H. 1993 Negative-temperature states and large-scale, long-lived vortices in two-dimensional turbulence. *J. Stat. Phys.,* **70**, 833–886.
[8]Caglioti, E., Lions, P. L., Marchioro, C., & Pulvirenti, M. 1992 A special class of stationary flows for two-dimensional Euler equations: a statistical mechanics description. *Comm. Math. Phys.,* **143**, 501–525.
[9]Lions, P. L., & Majda, A. J. 2000 Equilibrium statistical theory for nearly parallel vortex filaments. *Comm. Pure App. Math.,* **8**, 76–142.
[10]Weiss, J. B., & McWilliams, J. C. 1991 Nonergodicity of point vortices. *Phys. Fluids A,* **3**, 835–844.
[11]Weiss, J. B., Provenzale, A., & McWilliams, J. C. 1998 Lagrangian dynamics in high-dimensional point-vortex systems. *Phys. Fluids,* **10**, 1929–1941.
[12]Lamb, H. 1932 *Hydrodynamics, 6th ed.* Cambridge University Press, 738pp.
[13]Bühler, O., & Jacobson, T. E. 2001 Wave-driven currents and vortex dynamics on barred beaches. *J. Fluid Mech.,* **449**, 313–339.
[14]Chorin, A. J. 1994 *Vorticity and turbulence.* Springer, 174pp.